 doi:10.20944/preprints201901.0248.v1

Review

Multiple-layer microperforated panels as sound absorbers in buildings: a review

Pedro Cobo [1]*, and Francisco Simón [2]

[1] Institute for Physical and Information Technologies (ITEFI), Spanish National Research Council (CSIC), Serrano 144, 28006 Madrid, Spain; pedro.cobo@csic.es
[2] Institute for Physical and Information Technologies (ITEFI), Spanish National Research Council (CSIC), Serrano 144, 28006 Madrid, Spain; f.simon@csic.es
* Correspondence: pedro.cobo@csic.es; Tel.: +34-915618806

Abstract: Sound absorbing materials are used in building to dissipate sound energy into heat by viscous and thermal processes. Sound absorbers increase the transmission loss of walls, decrease the reverberation time of rooms and attenuate the noise generated by internal sound sources. Porous absorbers (fibrous, cellular or granular) are the most used materials in noise control applications, since their high performance-to-cost ratio in the frequency band of interest. However, when cleaning and health reasons are of concern, microperforated panel (MPP) absorbers can be preferred. MPPs, consisting of many minute (sub-millimetric) holes in a panel, are tunable absorbers in a prescribed frequency band, which main shortcomings are high manufacturing cost and limited absorption frequency band. Production cost of MPP can nowadays be drastically cut down by means of modern techniques. Absorption frequency band can be considerably enlarged by designing multiple-layer MPPs (ML-MPPs). The aim of this article is to review the high potential of ML-MPPs as a modern, clean and healthy alternative of porous materials for sound absorption.

Keywords: Sound absorption; microperforated panels; multilayer systems

1. Introduction

Porous and fibrous materials are excellent sound absorbers at a reasonable cost. They are used in most situations where sound must be dissipated, either for increasing the sound insulation of multilayer walls of buildings or, as liners, for decreasing the reflective characteristics of inner walls. However, porous and fibrous absorbers can potentially release particles which can become a trouble in environs requiring special cleaning and health conditions, such as alimentary industry, hospitals, or white rooms for production of microelectronic devices. Other applications where these materials are not recommended are inside of ducts circulated by high velocity gases, such as the exhaust of engines [1].

Maa [2-3] proposed an alternative absorbing material especially suited for these situations, the so named microperforated panels (MPP). The MPPs formerly proposed by Maa consisted of a distribution of minute circular holes of diameter d, over a panel of thickness t, with a perforation ratio, or porosity ϕ. This MPP has an acoustic impedance, Z, which is complex, i.e., has resistive a reactive components. This acoustic impedance need to be matched to the air impedance, Z_0, which is real, if the MPP must provide significant sound absorption. Hence, additional imaginary impedance is required to counteract the reactive part of Z. The necessary reactive impedance is provided by an air cavity of thickness D. Therefore, a single-layer MPP (SL-MPP) is obtained which depends on the parameter set (d,t,ϕ,D).

The absorption coefficient of a system can be easily calculated once the input impedance to the system is known. Two of the most prominent models for the acoustic impedance of an MPP are the Maa [2-3] and the equivalent fluid (EF) [4-6] models. The Maa model add to the impedance of a hole

Preprints (www.preprints.org) | NOT PEER-REVIEWED | Posted: 24 January 2019 doi:10.20944/preprints201901.0248.v1

first proposed by Crandall the edge impedance suggested by Ingard [7]. The EF model uses also the Crandall impedance for the holes but the edge impedance is introduced through the tortuosity, similar to that used in the modelling of porous materials.

A MPP appropriate for absorbing sound in the frequency band of interest in noise control applications might have hundreds of thousands holes per square meter. Formerly, these minute perforations were machined by laser technology, which was rather expensive. There were several proposals for reducing the manufacturing costs of MPPs. One of the first was perforating the panel in slits instead of holes, leading to the microslotted panels, or MSP [8-10].

Pfretzschner *et al.* [11] proposed combining the millimetric holes of a carrying plate with the micrometric perforations of a woven mesh to provide absorption performance similar to that of a MPP, obtaining the so named Microperforation Insertion Unit (MIU). Since the carrying plate could be machined by conventional drilling and commercial meshes could be added as micrometric meshes, the resulting MIU was significantly cheaper than the MPP with the same absorbing performance [12].

More recently Cobo and Montero de Espinosa [13] and Quian *et al.* [14] proposed alternative technologies to machining MPPs with reduced manufacturing cost. Cobo and Montero de Espinosa used an infiltration technique. They start with a mixing of polymeric material with salt grains of proper size and quantity. Once the mixing is cured, it is introduced into a water bath to remove the salt grains leaving irregular holes of sub-millimetric size. Quian *et al.* used a MEMS technology to machine MPPs with ultraperforations of diameter lower than 100 μm which afforded sound absorption in a bandwidth larger than that of conventional MPPs.

Therefore, SL-MPPs are structures able to provide clean sound absorption into a relatively narrow bandwidth (1-2 octaves). However, the frequency band of absorption can be increased by designing multiple-layer MPPs [15-17]. Whilst the design of a single-layer MPP depends on four parameters (d,t,ϕ,D), the tuning of a N-layer MPP depends on 4N parameters. Thus, optimization procedures must be used to adjust these multiple-layer MPPs [18].

The aim of this article is to review the different models and structures of MPPs as modern, clean and healthy materials for sound absorption.

2. SL-MPP

A SL-MPP consists of a panel of thickness t, with perforations of diameter d and porosity ϕ, in front of an impervious wall, leaving an air cavity of thickness D, Figure 1. Such a system is characterised by input impedance Z_1. When a plane wave propagating in air of characteristic impedance Z_0 finds this MPP system, the impedance contrast (Z_1-Z_0) causes a wave reflection, and as a consequence, produces sound absorption. At normal incidence, the reflection, R, and absorption, α_0, coefficients are

$$R = \frac{Z_1 - Z_0}{Z_1 + Z_0} \quad , \tag{1}$$

$$\alpha_0 = 1 - |R|^2 \quad . \tag{2}$$

The input impedance to the MPP, Z_1, contains four effects [19]:

- The visco-thermal dissipation within the holes, Z_{hole}.
- The distortion of flow in the perforation edges, Z_{edge}.
- The resonances in the air cavity, Z_c.
- The structural vibrations of the panel, Z_{vib}.

The joint contribution of Z_{hole} and Z_{edge} is the MPP impedance Z_{MPP}. The impedance of the air cavity is

$$Z_c = -iZ_0 cot(kD), \tag{3}$$

Preprints (www.preprints.org) | NOT PEER-REVIEWED | Posted: 24 January 2019 doi:10.20944/preprints201901.0248.v1

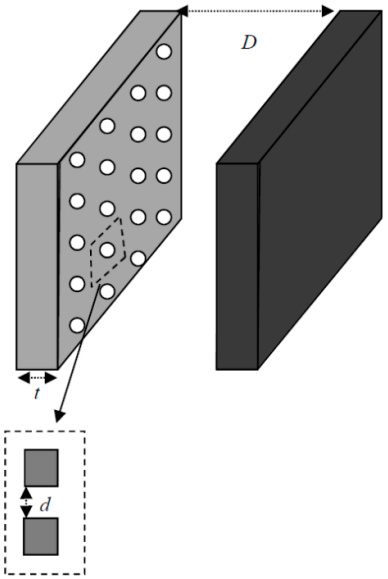

Figure 1. Sketch of a SL-MPP.

whre $k=\omega/c$ is the wavenumber, $\omega=2\pi f$ is the angular frequency, c is the sound velocity in air, and f is the frequency. The structural impedance of the panel, Z_{vib}, can be obtained from the elastic properties of the panel [20]. Therefore, the input impedance to the MPP system is

$$Z_1 = \frac{Z_{MPP}Z_{vib}}{Z_{MPP}+Z_{vib}} + Z_C \quad . \tag{4a}$$

For a rigid panel, $Z_{vib}\rightarrow\infty$, and

$$Z_1 = Z_{MPP} + Z_C \quad . \tag{4b}$$

The Maa and EF models for the MPP, Z_{MPP}, and more specifically, for the impedances of the perforations, Z_{hole}, and edges, Z_{edge}, will be reviewed in the following.

2.1. Maa Model

Maa [3] assumed the perforations impedance, Z_{hole}, deduced from the solution of the wave equations in a cyllindrical tube proposed formerly by Rayleigh and solved then by Crandall for short tubes

$$i\omega\rho_0 u = \frac{\eta}{r_1}\frac{\partial}{\partial r_1}\left(r_1\frac{\partial u}{\partial r_1}\right) + \frac{\Delta p}{t} \quad , \tag{5}$$

where u is the particle velocity in the tube, r_1, is the radial coordinate in the tube, η is the air viscosity, and Δp is the presuure difference at both sides of the tube. Solving for u, and averaging on the tube surface, the following equantion is otained

$$\bar{u} = -\frac{1}{i\omega\rho_0}\left[1 - \frac{2}{s\sqrt{-i}}\frac{J_1(s\sqrt{-i})}{J_0(s\sqrt{-i})}\right]\frac{\Delta p}{t} \, , \tag{6}$$

which affords for the hole impedance $Z_{hole} = -\Delta p/\bar{u}$,

$$Z_{hole} = i\omega\rho_0 t\left[1 - \frac{2}{s\sqrt{-j}}\frac{J_1(s\sqrt{-i})}{J_0(s\sqrt{-i})}\right]^{-1} \, , \tag{7a}$$

with

$$s = d\sqrt{\frac{\rho_0\omega}{4\eta}} = r\sqrt{\frac{\rho_0\omega}{\eta}} \quad , \tag{8}$$

Preprints (www.preprints.org) | NOT PEER-REVIEWED | Posted: 24 January 2019 doi:10.20944/preprints201901.0248.v1

being ρ_0 the air density, η the air viscosity, ω the angular frequency, $r=d/2$ the perforation radius, and J_0 and J_1 the Bessel functions of first class and orders 0 and 1, respectively. To extrapolate this solution to that of a MPP it is neccessary to take into account the relationship between the particle velocity inside and outside the perforations, Figure 2 [21-22]. Hence

$$Z_{hole} = \frac{-\Delta p}{u'} = i\frac{\omega\rho_0}{\phi} t\left[1 - \frac{2}{s\sqrt{-j}}\frac{J_1(s\sqrt{-i})}{J_0(s\sqrt{-i})}\right]^{-1}. \quad (7b)$$

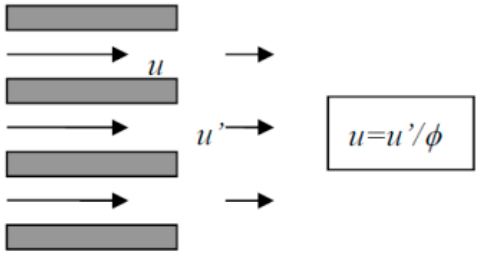

Figure 2. Relationship between the particle velovity inside, u, and outside, u', the perforations of a MPP.

The variable s in Eq. (8) represents the ratio of the diameter of the perforations to the boundary layer thickness. Strictily speaking, Maa [2] used an approximation of Eq. (7b) for Z_{hole} valid in the range $1<s<10$. Nevertheless, the exact version of Eq. (7b) will be used in this article.

Maa [3] considered a Z_{edge} term composed of two terms, one resistive, due to the friction of the air flow in the edges of the holes, and other reactive, due to the piston-like radiation of the air at both edges. The resistive term is named also surface resistance, R_s. The reactive term is named mass reactance, X_m. Thus

$$Z_{edge} = R_s + iX_m = \frac{\sqrt{2\eta\omega\rho_0}}{2} + i\omega\rho_o 0.85d \ . \quad (9a)$$

According to Hou [23] and Tayong *et al.* [20], the resistive term in Eq. (9a) should be 4 times higher

$$Z_{edge} = R_s + iX_m = 2\sqrt{2\eta\omega\rho_0} + i\omega\rho_o 0.85d \ . \quad (9b)$$

These are the resistive and reactive terms used in most MPP models and will be also assumed in this article. Notice that

$$2\sqrt{2\mu\omega\rho_0} = 2\sqrt{2}\mu\sqrt{\frac{\omega\rho_0}{\eta}} = 2\sqrt{2}\frac{s}{d} \ . \quad (10)$$

The reactive term can be also interpreted as an excess of vibrating mass, $2\delta = 0.85\ d$, Figure 3, where a multiplying factor of 2 is used to take into account both sides of the hole.

The edge impedance of Eq. (9) assumes that the perforations are separated enough from each other (low perforation ratio ϕ) so that there is not edge interaction effects. However, these interactions can become significant when the holes are close each others. Melling [24] proposed to take into consideration edge effects by modifying the reactive part, X_m, as follows

$$X_m = i\omega\rho_0 \frac{0.85\ d}{F(\epsilon)} \ , \quad (11)$$

being

$$F(\epsilon) = (1 - 1.4092\ \epsilon + 0.33818\ \epsilon^3 + 0.06793\ \epsilon^5 - 0.02287\ \epsilon^6 + 0.03015\epsilon^7 - 0.01641\epsilon^8)^{-1}, \quad (12)$$

the Fok function. Melling [24] and Rschevkin [25] used $\epsilon = d/D$, where $D = 2\sqrt{S/\pi}$, and S is the area of the edge effects (shaded area in Figure 4).

Preprints (www.preprints.org) | NOT PEER-REVIEWED | Posted: 24 January 2019 doi:10.20944/preprints201901.0248.v1

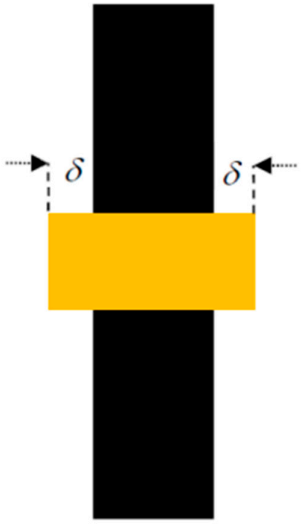

Figure 3. Mass reactance due to the excess of vibrating mass in the hole edges.

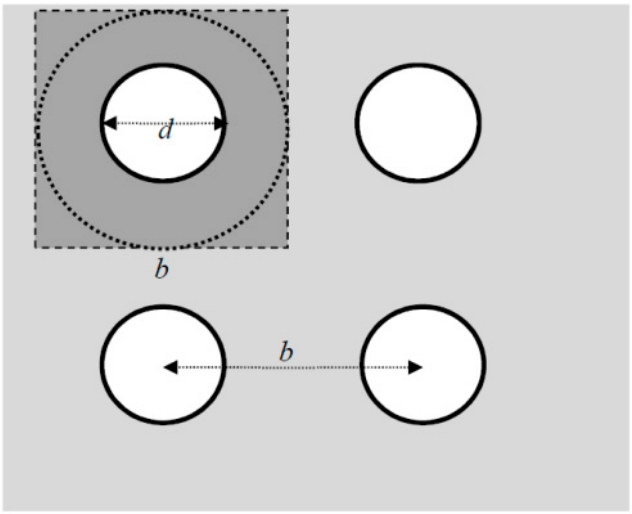

Figure 4. Meaning of b and d in the definition of ϵ for the Fok function.

Randeberg [9] and Tayong and Leclaire [20], on the other hand, define $\epsilon = d/b$, where b is the separation between holes in an uniform distribution, Figura 4. Both definitions coincide if $D=b$. Furthermore, taking into account that $\phi = (\pi/4)(d/b)^2$ [2], ϵ can be also be set as a function of ϕ, $\epsilon = \frac{d}{b} = \frac{2}{\sqrt{\pi}}\sqrt{\phi} = 1.1284\sqrt{\phi}$. Other authors [25], use the relation $\epsilon = \sqrt{\phi}$ which will be used in this article. Figure 5 shows the Fok function (correction factor of the mass reactance) as a function of porosity. As it can be seen, the correction factor is small for low porosity values, but begins to be significant for porosities higher than 2%. Since this factor corrects the length excess of the oscillating mass in the holes, the effect of overperforaton is to cut out this length excess.

Therefore, the Maa model with overperforation effects provides the following equation for the input impedance to a SL-MPP

$$Z_{1,Maa} = \frac{\sqrt{2\rho_0\omega\eta}}{2\phi} + i\frac{\omega\rho_0}{\phi}\left\{0.85\,\frac{d}{F(\epsilon)} + t\left[1 - \frac{2}{s\sqrt{-j}}\frac{J_1(s\sqrt{-i})}{J_0(s\sqrt{-i})}\right]^{-1}\right\} - iZ_0 cot(kD). \quad (13)$$

The normal incidence absorption coefficient, which can be calculated by introducing this Eq. (13) into the Eqs. (1) and (2), depends on the four constitutive parameters (d,t,ϕ,D) of the SL-MPP.

Preprints (www.preprints.org) | NOT PEER-REVIEWED | Posted: 24 January 2019 doi:10.20944/preprints201901.0248.v1

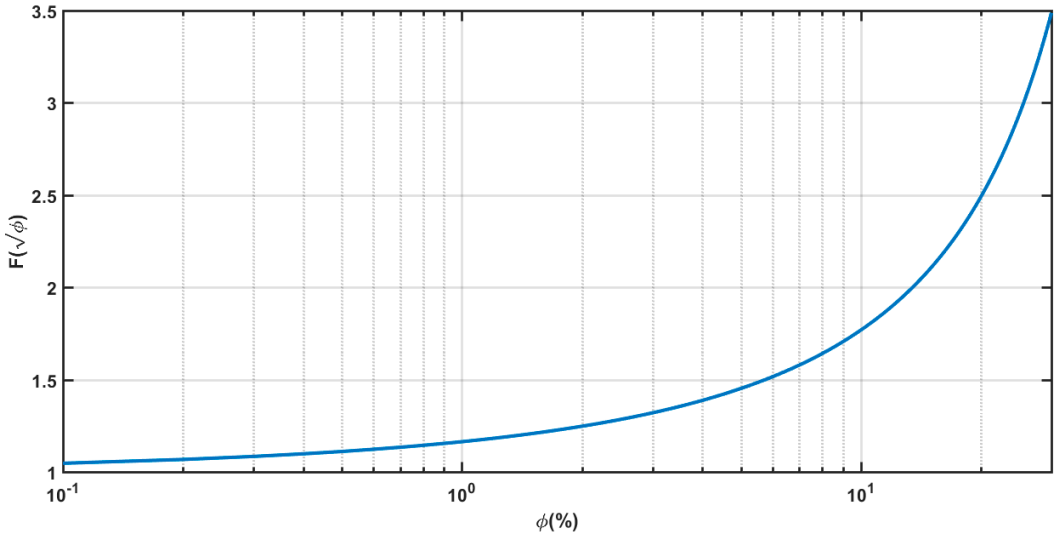

Figure 5. Graphical representation of the Fok function.

Figures 6-9 show the absortion coefficient as a function of one of these parameters, keeping constant the other three. From these Figures, the following can be assessed:

- For each combination of (t,ϕ,D) there exist a value of d providing maximum absorptiion. Furthermore, the absorption bandwidth increases as d decreases.
- For each combination of (d,ϕ,D) there is a value of t yielding maximum absorption. The absorption curve moves towards higher (lower) frequencies as t decreases (increases).
- Keeping constant the combination of parameters (d,t,D), there is a value of ϕ affording maximum absorption. The absorption curve moves towards higher frequencies, and the absorption bandwith increases, as ϕ increases.
- Keeping constat the combination of parameters (d,t,ϕ), the effect of D is to move the absorption curve towards lower freqiencies as D increases.

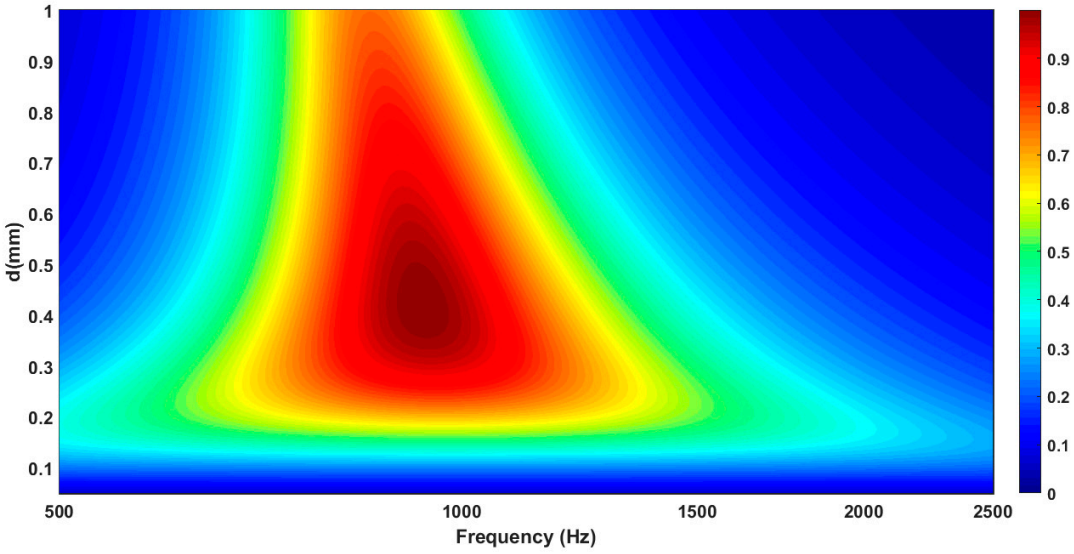

Figure 6. Absorption coefficient of a SL-MPP as a function of (f,d) for (t,ϕ,D)=(1 mm,1%,2 cm).

Preprints (www.preprints.org) | NOT PEER-REVIEWED | Posted: 24 January 2019 doi:10.20944/preprints201901.0248.v1

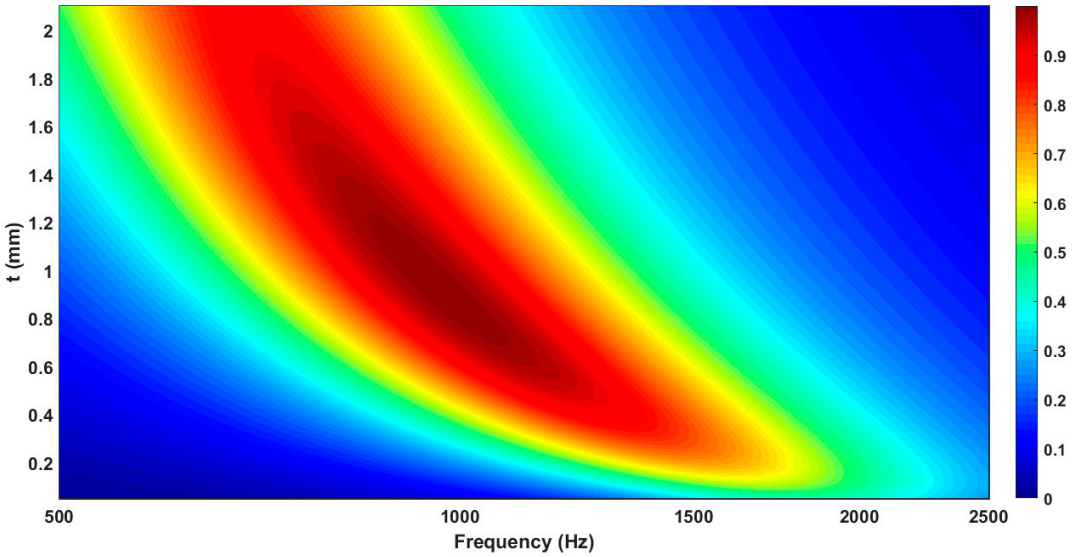

Figure 7. Absorption coefficient of a SL-MPP as a function of (f,t) for (d,ϕ,D)=(0.4 mm,1%,2 cm).

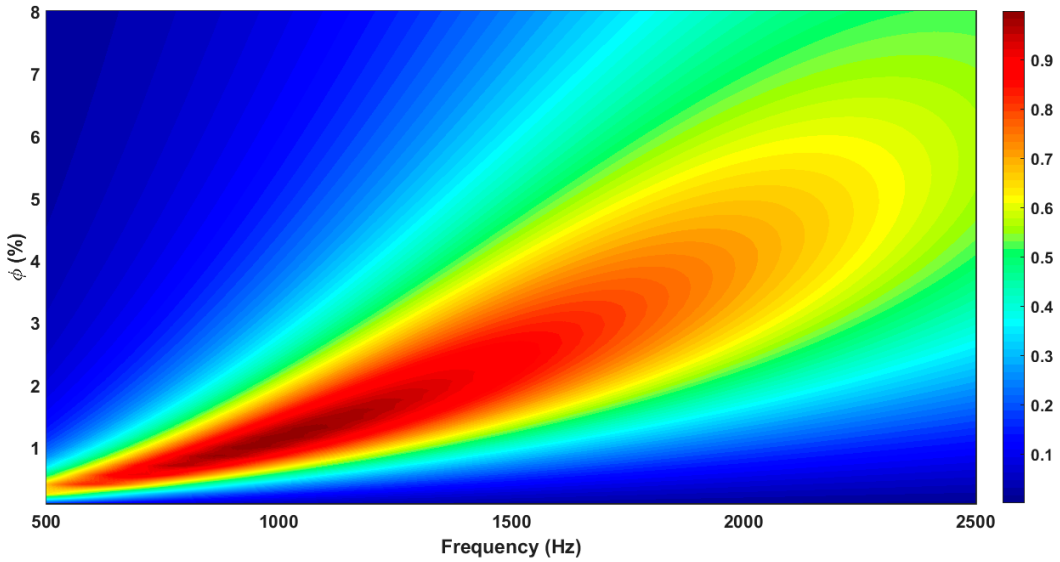

Figure 8. Absorption coefficient of a SL-MPP as a function of (f,ϕ) for (d,t,D)=(0.4 mm,1 mm,2 cm).

Maa [2] proposed designing SL-MPPs with d=t. As it is seen in Figure 10, which dispalys the absorption coefficient of a SL-MPP as a function of (d,t) for f=1500 Hz, ϕ=1% and D= 2 cm, this is a reasonable guess.

Figure 11 shows the absorption curves of a SL-MPP as a function of frequency, for t=0.5 mm, D= 2 cm and different values of the other two parameters. As it can be seen, a SL-MPP provides sound absorption in a frequency band of 1-2 octaves. The absorption bandwidth is the interval (f_i,f_s), where f_i and f_s are the frequencies at half absorption at each side of the peak. The number of octaves spanned is

$$N_{octaves} = \frac{log(f_s/f_i)}{log(2)} \quad . \tag{14}$$

Preprints (www.preprints.org) | NOT PEER-REVIEWED | Posted: 24 January 2019 doi:10.20944/preprints201901.0248.v1

The absorption bandwidth increases considerably reducing the hole diameter, provided that the porosoty is also increased, although the absorption curve is moved towards higher frequencies, as pointed out by Quian *et al.* [14].

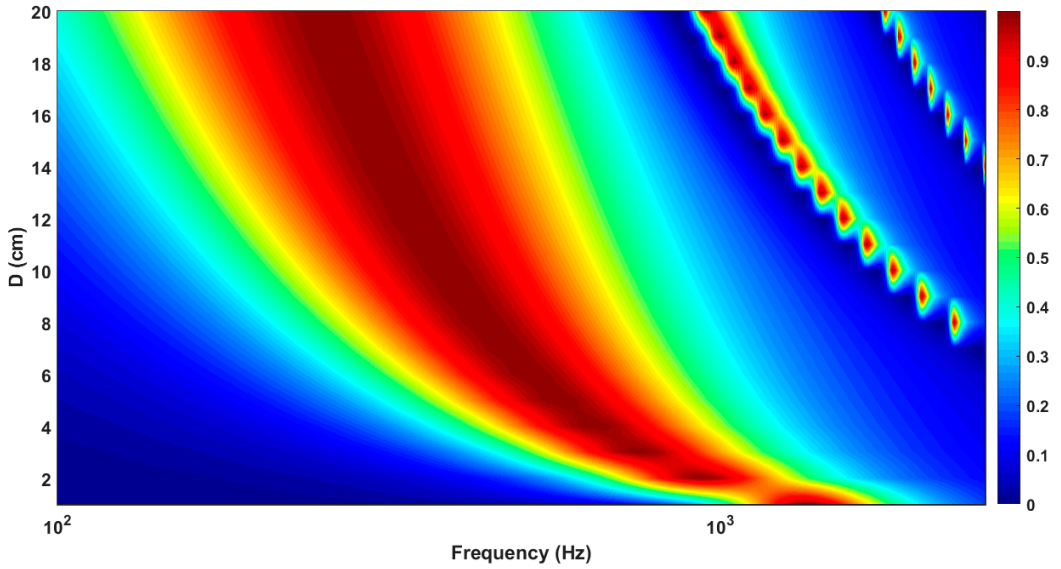

Figure 9. Absorption coefficient of a SL-MPP as a function of (f,D) for (d,t,ϕ)=(0.4 mm,1 mm,1 %).

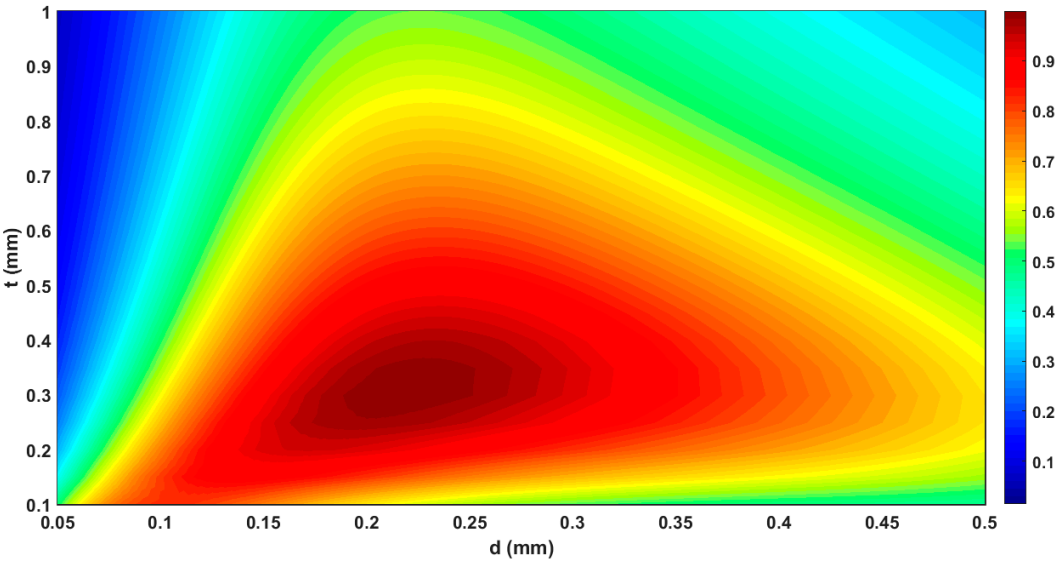

Figure 10. Absorption coefficient of a SL-MPP as a function of (d,t) for (f,ϕ,D)=(1500 Hz,1%, 2 cm).

Preprints (www.preprints.org) | NOT PEER-REVIEWED | Posted: 24 January 2019 doi:10.20944/preprints201901.0248.v1

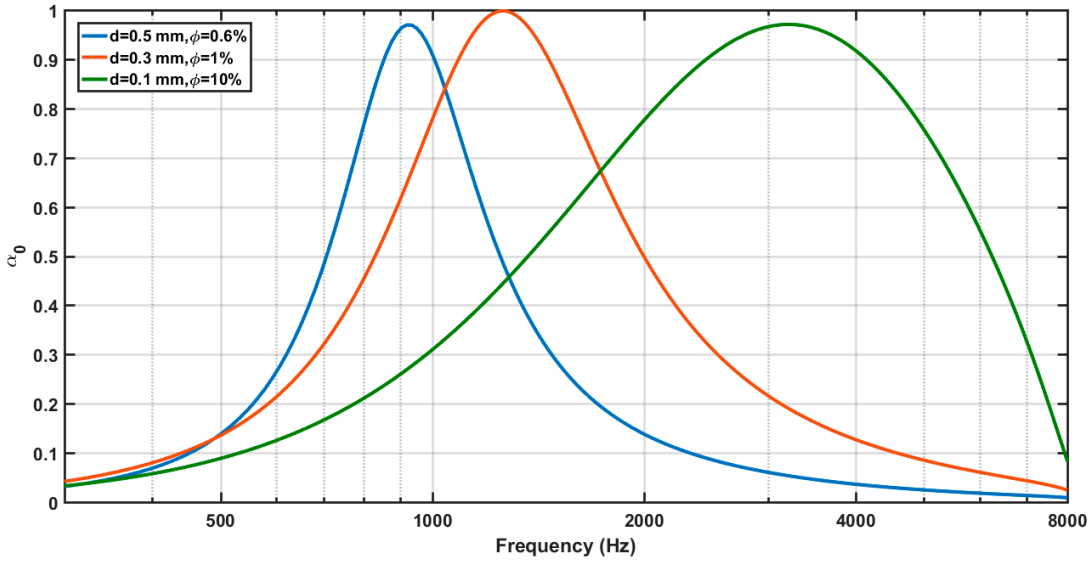

Figure 11. Absorption coefficient of a SL-MPP with t=0.5 mm, D=2 cm and different values of d and ϕ.

2.2. EF Model

Atalla and Sgard [6] proposed an equivalent fluid (EF) model of a SL-MPP, based on the Johnson-Champoux-Allard model for porous materials [4-5]. In this model, it is assumed a perforated panel of infinite lateral dimension coupled at both sides to a semi-infinite fluid. The impedance of such a panel has resistive and reactive components. The resistive part is induced by the viscous effects in the perforations, due to the viscous boundary layer, and around the edges of the holes, due to the distortion of the flow. The reactive part takes into account the movement of the air cylinder of length larger than the panel thickness. It is due to the load of the mass associated to the sound radiation of the panel, which contributes to make the air mass associated to the hole neck heavier and more difficult to move. This inertial effect contributes to increase the vibrating air mass and is taken into account using a length correction that must be added to the perforation length, t. Atalla y Sgard [6] demonstrated that the EF model predicts the following equation for the hole impedance

$$Z_{hole} = i\omega\tilde{\rho}_e \frac{t}{\phi} \quad , \tag{15a}$$

where $\tilde{\rho}_e$, the effective density, is

$$\tilde{\rho}_e = \rho_0 \left[1 + \frac{\sigma p G_J(\omega)}{i\omega\rho_0}\right] \quad , \tag{15b}$$

$$G_J(\omega) = \left(1 + i\frac{4\omega\rho_0\eta}{\sigma^2\phi^2 r^2}\right)^{1/2}, \tag{15c}$$

being

$$\sigma = \frac{8\eta}{\phi r^2} \quad , \tag{15d}$$

the flow resistivity, η the air dynamic viscosity, and r=d/2 the hole radius. Since this formulation is valid for the whole frequency range, it is valid for both micro (MPP) and macro (screens) perforations [6].

The edge effects are introduced in the EF model through the geometric tortuosity, α_∞, defined as the high frequency limit of the tortuosity $\tilde{\alpha}_e = \tilde{\rho}_e/\rho_0$. In porous materials, the geometrical tortuosity takes into account the relative increase of density of the ideal non viscous fluid filling the rigid skeleton [4-5]. Stinson y Champoux [26] defined the geometrical tortuosity also as the ratio of the pores length to the thickness of the panel. For a SL-MPP with evenly distributed perforations of

Preprints (www.preprints.org) | NOT PEER-REVIEWED | Posted: 24 January 2019 doi:10.20944/preprints201901.0248.v1

angle θ, the geometrical tortuosity is simply α_∞ =1/cos θ. Therefore, it is an intrinsic parameter of the absorbing material which depends on its micro-geometry. The geometrical tortuosity of a SL-MPP depends also on the media in contact with the panel. For the case of a panel radiating to both sides [6]

$$\alpha_\infty = 1 + \frac{2\epsilon_e}{t} \quad , \tag{16a}$$

with

$$\epsilon_e = \epsilon_0\left(1 - 1.14\sqrt{\phi}\right) \quad , \tag{16b}$$

being $\epsilon_0 = 0.48\sqrt{\pi r^2} = 0.85r$, and ϕ<0.4. This tortuosity takes into account the length correction of the air vibrating to both sides of the holes (hence the factor 2 in the numerator of the second term of Eq. (16a)). The term in brackets in Eq. (16b) includes the edge interaction between close perforations, and plays here the same role than the Fok function introduced by Melling [24].

Jaouen and Becot [19] used the EF model to characterise acoustic screens (low frequency, large holes approach). They employed the following overperforation correction function

$$F(\epsilon) = (1 - 1.13\epsilon - 0.09\epsilon^2 + 0.27\epsilon^3)^{-1}, \tag{17}$$

with $\epsilon = \sqrt{\phi}$. As it can be seen in Figure 12, both functions do not differ so much in the range ϕ<30%.

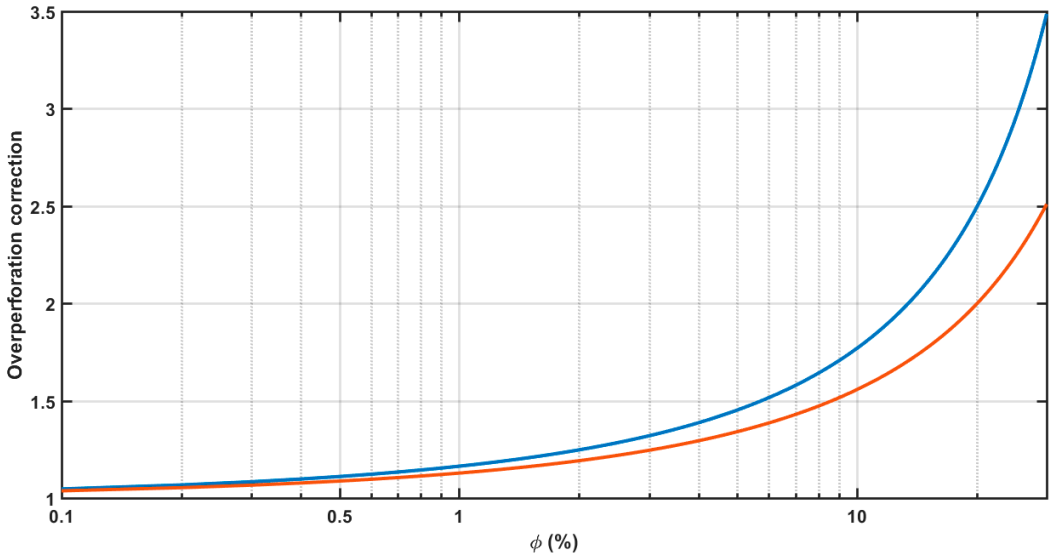

Figure 12. Overperforation correction factors by Fok function and tortuosity.

It is worth to emphasize that the edge effects in the EF model are introduced through the tortuosity as a multiplicative factor, unlike the Maa model, where it was included as an additive term. Thus, the panel impedance for a MPP in the EF model is

$$Z_{MPP,EF} = i\frac{\omega\rho_0\alpha_\infty t}{\phi}\left[1 + \frac{\sigma\phi}{i\rho_0\omega\alpha_\infty}\left(1 + i\frac{4\omega\rho_0\alpha_\infty^2\eta}{\sigma^2\phi^2r^2}\right)^{1/2}\right], \tag{18}$$

and the input impedance to a SL-MPP is

$$Z_{1,FE} = i\frac{\omega\rho_0\alpha_\infty t}{\phi}\left[1 + \frac{\sigma\phi}{i\rho_0\omega\alpha_\infty}\left(1 + i\frac{4\omega\rho_0\alpha_\infty^2\eta}{\sigma^2\phi^2r^2}\right)^{1/2}\right] - iZ_0cot(kD) \ . \tag{19}$$

2.3. Comparison Between Maa and EF Models

Figure 13 shows the absorption curves provided by the Maa and EF models for *D*=3 cm and three combinations of (d,t,ϕ) parameters, using the overperforation correction provided by the Fok

Preprints (www.preprints.org) | NOT PEER-REVIEWED | Posted: 24 January 2019 doi:10.20944/preprints201901.0248.v1

function in both models. The first combination of parameters (d,t,ϕ,D)=(0.5 mm,0.5 mm,0.5%,3 cm) corresponds to a SL-MPP with low perforation ratio and 0.5 mm hole diameter. In this case, the EF model provides an absorption curve slightly displaced towards lower frequencies. The second SL-MPP corresponds to (d,t,ϕ,D)=(0.25 mm,1 mm,5%,3 cm). In this case, both curves are very similar, except for a slightly higher peak absoption of the Maa model. The third combinations of parameters (d,t,ϕ,D)=(0.15 mm,1.3 mm,10%,3 cm) stands for a overperforated SL-MPP. In this case both the Maa and the EF models provide absorption curves almost identical. Notice that the absorption bandwidth increases in comparison with that of the second example.

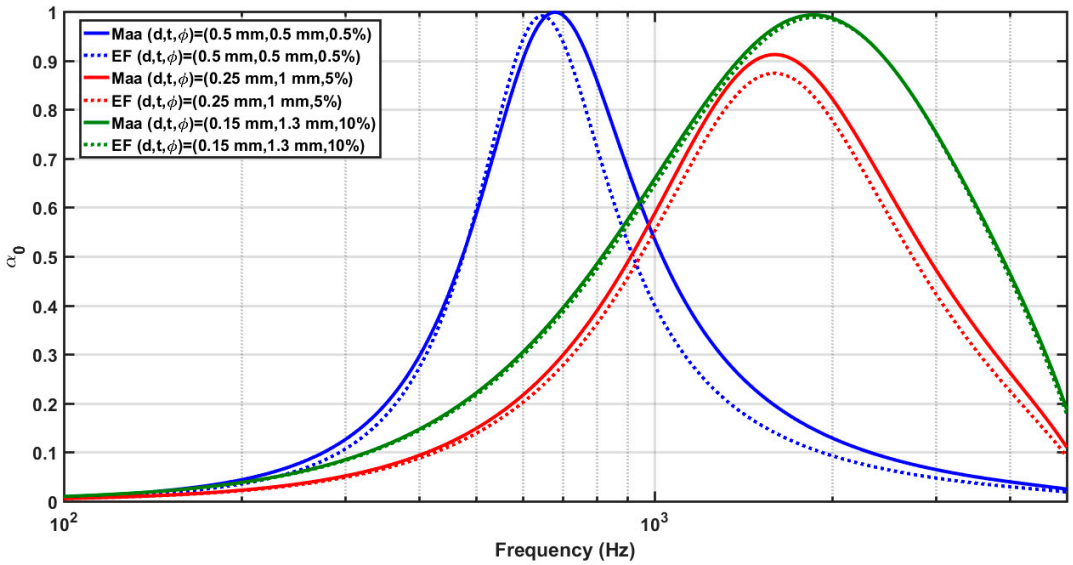

Figure 13. Absorption curves provided by the Maa (solid line) and EF (dotted line) models for D=3 cm and different combinations of the parameters (d,t,ϕ).

SL-MPPs provide absorption curves with a typical resonant shape. The low frequency limitation is due to the quarter wavelength condition of the air cavity. Low frequency absorption can be achieved by combining a MPP with an active control system, thus obtaining the so named hybrid passive-active absorption systems [27-30].

2.4. Microslotted Panels (MSP)

The impedance of perforations, Z_{hole}, depends on the geometry of holes. The Maa formulation [2-3], valid for circular holes, Figure 14a, includes Bessel functions. The equation of Z_{hole} for slits, Figure 14b, contains the hyperbolic tangent function [8-10]. The edge impedance also changes for slotted perforations [8-9]. The impedance of a SL-MSP of thickness t and hydraullic diameter d, is [9-10]

$$Z_{MSP} = \frac{i\omega\rho_0 t}{\phi}\left\{\left[1-\frac{\tanh(s\sqrt{i})}{s\sqrt{i}}\right]^{-1} - \frac{2d}{\pi t} ln\left[sin\left(\frac{\pi\phi}{2}\right)\right] - i\frac{d_v}{t}\right\}, \quad (20a)$$

where $s = d\sqrt{\rho_0\omega/4\eta}$ and $d_v = \sqrt{2\eta/\rho_0\omega}$ is the boundary layer thickness. According to Randeberg [9], Eq. (19a) already contains the effect of edge interaction. Therefore, the input impedance to a SL-MSP is

$$Z_{1,MSP} = \frac{i\omega\rho_0 t}{\phi}\left\{\left[1-\frac{\tanh(s\sqrt{i})}{s\sqrt{i}}\right]^{-1} - \frac{d}{\pi t} ln\left[sin\left(\frac{\pi\omega}{2b}\right)\right] - i\frac{d_v}{t}\right\} - iZ_0\cot(kD)\ . \quad (20b)$$

Preprints (www.preprints.org) | NOT PEER-REVIEWED | Posted: 24 January 2019 doi:10.20944/preprints201901.0248.v1

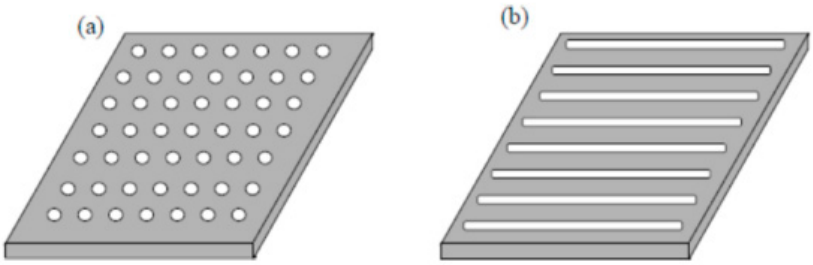

Figure 14. Sketch of a panel microperforated with (a) circular holes and (b) slits.

Maa [8] provided different equations for the impedance of a MSP, namely

$$Z_{MSP} = R + i\chi, \tag{21a}$$

where

$$R = \frac{12\eta t}{\phi d^2}\left(\sqrt{1+\frac{s^2}{18}+\frac{\sqrt{2}sd}{12t}}\right), \tag{21b}$$

$$\chi = \frac{\rho_0 \omega t}{\phi}\left[1+\frac{1}{\sqrt{25+2y^2}}+\frac{F(e)d}{2t}\right], \tag{21c}$$

$$F(e) = \frac{\pi}{2}\left[\left(\frac{1}{2}\right)^2 e^2 + \left(\frac{1\cdot 3}{2\cdot 4}\right)^4 e^4 + \left(\frac{1\cdot 3\cdot 5}{2\cdot 4\cdot 6}\right)^6 e^6 + \cdots\right], \tag{21d}$$

$$e = \sqrt{1-\left(\frac{d}{l}\right)^2}, \tag{21e}$$

with $s = d\sqrt{\rho_0\omega/4\eta}$, and l the slit length. Adding the air cavity impedance, the Maa impedance of the SL-MSP is obtained

$$Z_{1,MSP-Maa} = \frac{12\eta t}{\phi d^2}\left(\sqrt{1+\frac{s^2}{18}+\frac{\sqrt{2}sd}{12t}}\right) + \frac{i\rho_0\omega t}{\phi}\left[1+\frac{1}{\sqrt{25+2y^2}}+\frac{F(e)d}{2t}\right] - iZ_0\cot(kD)\ . \tag{22}$$

Figure 15 shows a comparison of the absorption curves of a SL-MSP and an equivalent Maa SL-MPP (this latter with the same hydraulic diameter and the same perforation ratio) for (d,t,ϕ,D)=(0.15 mm,1 mm,5%,5 cm). For this combination of parameters, the SL-MPP provides more absorption than the SL-MSP, in a wider frequency band. However, as it can be seen in Figure 16, the comparison of the acoustic performance of SL-MSP and equivalent SL-MPP will depend on the combination of parameters. In all the cases, the equivalent SL-MPP always provides more absorption than the SL-MSP.

Preprints (www.preprints.org) | NOT PEER-REVIEWED | Posted: 24 January 2019 doi:10.20944/preprints201901.0248.v1

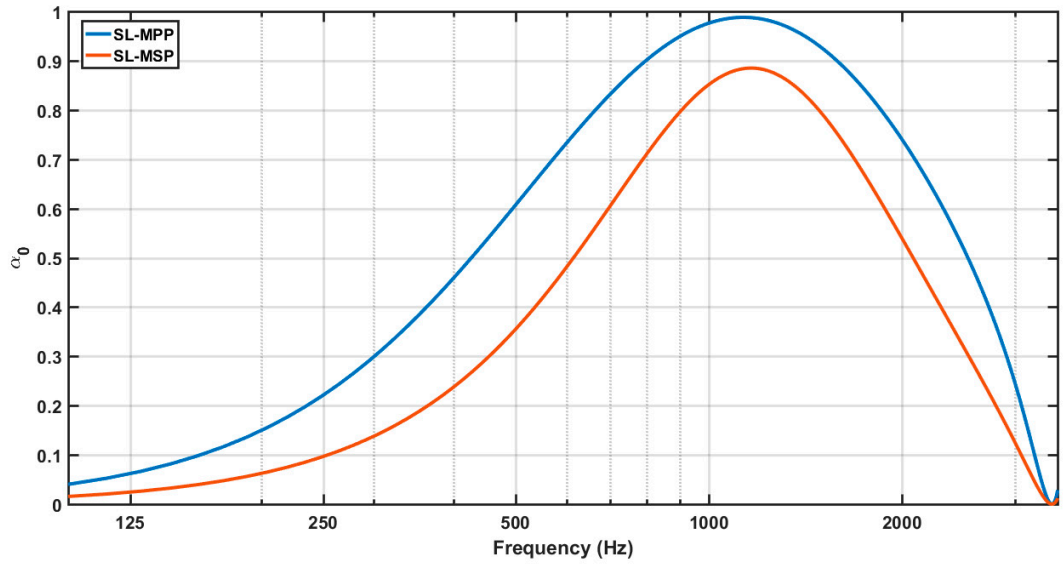

Figure 15. Comparison of the absorption curves of a SL-MSP and an equivalent SL-MPP for (d,t,ϕ,D)=(0.15 mm,1 mm,5%,5 cm).

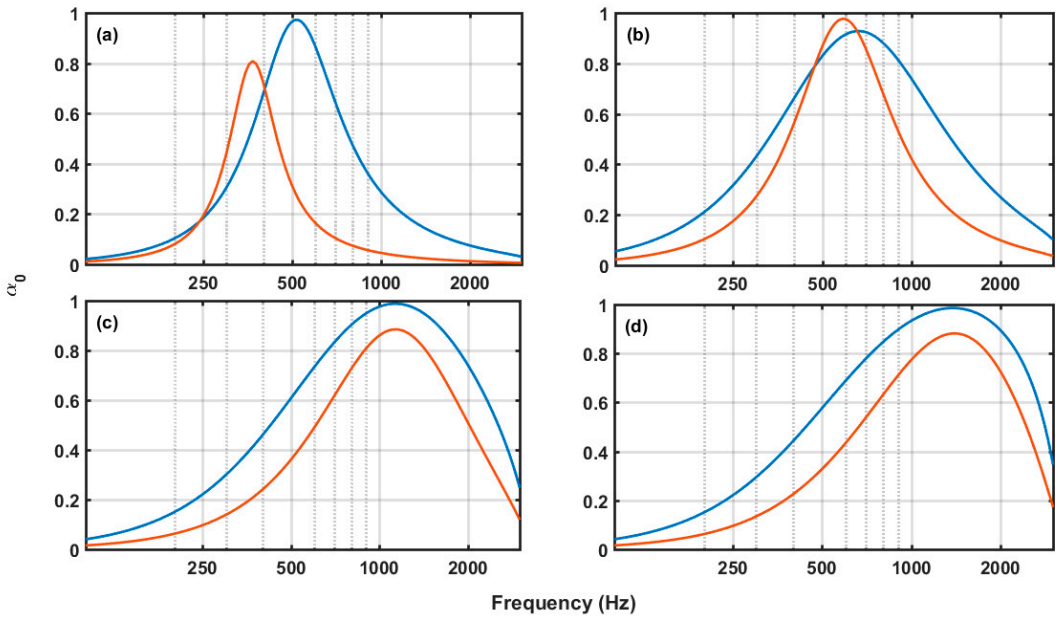

Figure 16. Absorption curves of an SL-MSP (red lines) and the equivalent SL-MPP (blue lines) for D=5 cm and (a) (d,t,ϕ)=(0.5 mm,0.5 mm,0.5%), (b) (d,t,ϕ)=(0.25 mm,0.75 mm,1%), (c) (d,t,ϕ)=(0.15 mm,1 mm,5%), and (c(d,t,ϕ)=(0.1 mm,1.13 mm,10%).

2.5. Microperforated Insertion Units (MIU)

The former MPPs used to be machined by laser technology and their cost was, therefore, expensive. Pfretzschner *et al.* [11] proposed a cheaper absorber, named Microperforated Insertion Unit (MIU), which combined two panels, one of them the carrying panel with millimetric holes, and other with micrometric hole diameter and thickness (Figure 17). The millimetric holes could be machined by conventional drilling and commercial filtering meshes could be used as the second micrometric plate.

Preprints (www.preprints.org) | NOT PEER-REVIEWED | Posted: 24 January 2019 doi:10.20944/preprints201901.0248.v1

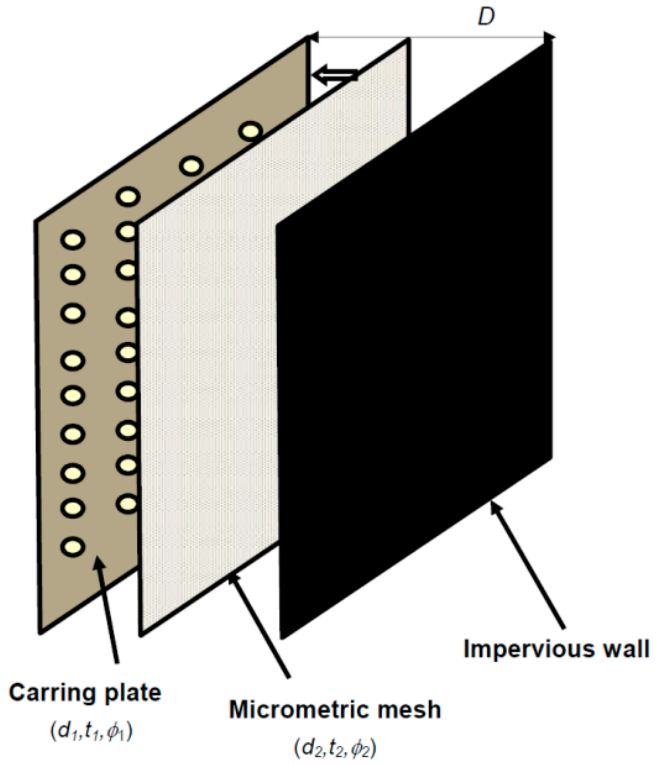

Figure 17. Sketch of a MIU.

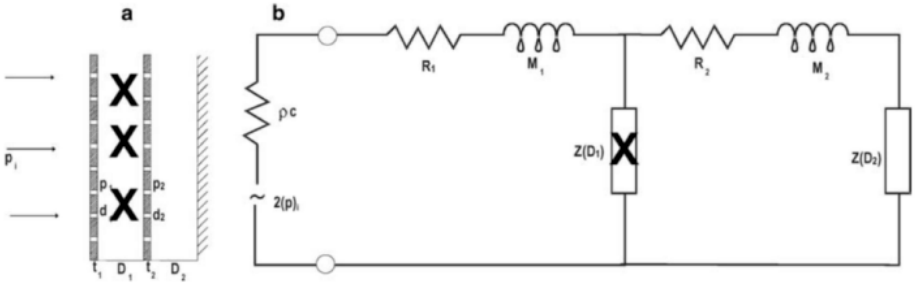

Figure 18. Equivalent circuit of a MIU.

Pfretzschner *et al.* [11] applied the equivalent circuit technique to obtain the input impedance of such a MIU (Figure 18). According to this model, the impedance of a MIU was

$$Z_{MIU} = Z_{m1} + Z_{m2} + Z_c \quad , \tag{23}$$

where Z_{m1} *and* Z_{m2} are the impedances of each of the panels (the carrying plate and the micrometric mesh), and Z_c is the air cavity impedance. Eq. (23) allows obtaining the absorption curve of the MIU, once Z_{m1} and Z_{m2} are set. For the Maa model, the SL-MIU impedance is [11]

$$Z_{1,MIU-Maa} = \frac{\sqrt{2\rho_0\omega\eta}}{2\phi_1} + i\frac{\omega\rho_0}{\phi_1}\left\{0.85\,\frac{d_1}{F(\epsilon_1)} + t_1\left[1 - \frac{2}{s_1\sqrt{-j}}\frac{J_1(s_1\sqrt{-i})}{J_0(s_1\sqrt{-i})}\right]^{-1}\right\}$$

$$+\frac{\sqrt{2\rho_0\omega\eta}}{2\phi_2} + i\frac{\omega\rho_0}{\phi_2}\left\{0.85\,\frac{d_2}{F(\epsilon_2)} + t_2\left[1 - \frac{2}{s_2\sqrt{-j}}\frac{J_1(s_2\sqrt{-i})}{J_0(s_2\sqrt{-i})}\right]^{-1}\right\} - iZ_0cot(kD) \quad , \tag{24a}$$

with

Preprints (www.preprints.org) | NOT PEER-REVIEWED | Posted: 24 January 2019 doi:10.20944/preprints201901.0248.v1

$$s_{1,2} = d_{1,2}\sqrt{\frac{\rho_0\omega}{4\eta}} \quad , \tag{24b}$$

and $\epsilon_{1,2} = \sqrt{\phi_{1,2}}$. Therefore, the absorption curve of a SL-MIU depends on 7 parameters (d_1,t_1,ϕ_1,d_2,t_2,ϕ_2,D).

This formulation does not take into account the effect in the interface between the carrying plate and the micrometric mesh. In fact, in this formulation, the boundary condition in this interface is just taken into consideration in the porosity of the micrometric mesh, which is $\phi_2' = \phi_2.\phi_1$. However, the flow modification across this interface might contribute to both the resistive and reactive parts of the edge impedance. The EF model allows introducing these edge effects easily, Figure 19.

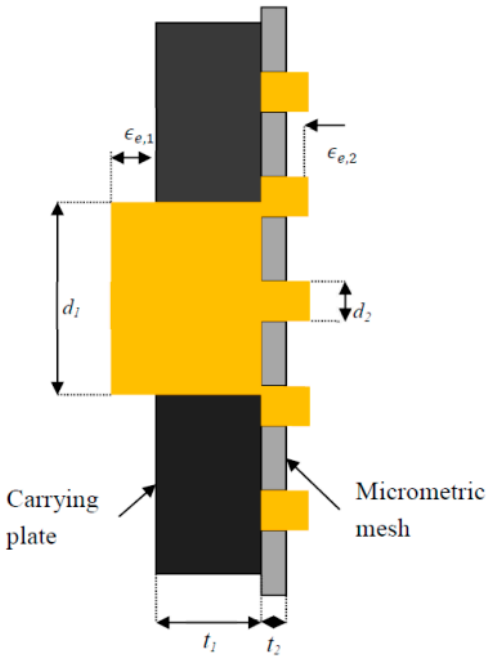

Figure 19. Boundary conditions at the MIU interface.

Let t_1 and t_2 be the thicknesses of both plates perforated with holes of diameters d_1 and d_2 and porosities ϕ_1 and ϕ_2, respectively. In the EF model, the edge effects are introduced through the tortuosities of both panels. For a SL-MPP, the geometrical tortuosity was given by Eq. (15a), $\alpha_\infty = 1 + (2\epsilon_e/t)$, being ϵ_e the excess of length of the vibrating air mass at each side of the holes. In this case, assuming continuity across the interface between the two plates, Figure 19, the tortuosities at both sides of the panels should be

$$\alpha_{\infty,2} = 1 + \frac{\epsilon_{e,2}}{t_2} \quad . \tag{25a}$$

and

$$\alpha_{\infty,1} = 1 + \frac{\epsilon_{e,1}}{t_1} \quad . \tag{25b}$$

The EF model impedance of a SL-MIU is therefore

$$Z_{1,MIU-EF} = i\omega\rho_0 \left\{ \alpha_{\infty,1}\frac{t_1}{\phi_1}\left[1 + \frac{\sigma_1\phi_1}{i\rho_0\omega\alpha_{\infty,1}}\left(1 + i\frac{4\omega\rho_0\alpha_{\infty,1}^2\eta}{\sigma_1^2\phi_1^2r_1^2}\right)^{1/2}\right] \right.$$
$$\left. + \alpha_{\infty,2}\frac{t_{21}}{\phi_2}\left[1 + \frac{\sigma_2\phi_2}{i\rho_0\omega\alpha_{\infty,2}}\left(1 + i\frac{4\omega\rho_0\alpha_{\infty,2}^2\eta}{\sigma_2^2\phi_2^2r_2^2}\right)^{1/2}\right] \right\} - iZ_0cot(kD)$$

Preprints (www.preprints.org) | NOT PEER-REVIEWED | Posted: 24 January 2019 doi:10.20944/preprints201901.0248.v1

(26a)

where

$$\sigma_{1,2} = \frac{8\eta}{\phi r_{1,2}^2} \quad , \tag{26b}$$

and $r_{1,2}=d_{1,2}/2$.

Figure 20 shows the absorption curves provided by the Maa and EF models for a SL-MIU with parameters (d_1,t_1,ϕ_1,d_2,t_2,ϕ_2,D)=(3 mm,1 mm,10%,41 μm,50 μm,31%,3 cm). As it can be seen the high frequency branch of the absorption curve provided by the EF model is slightly displaced towards higher frequencies, as compared with the Maa model curve. A SL-MIU provides an absorption curve similar to that of a SL-MPP with a bandwidth of 1-2 octaves.

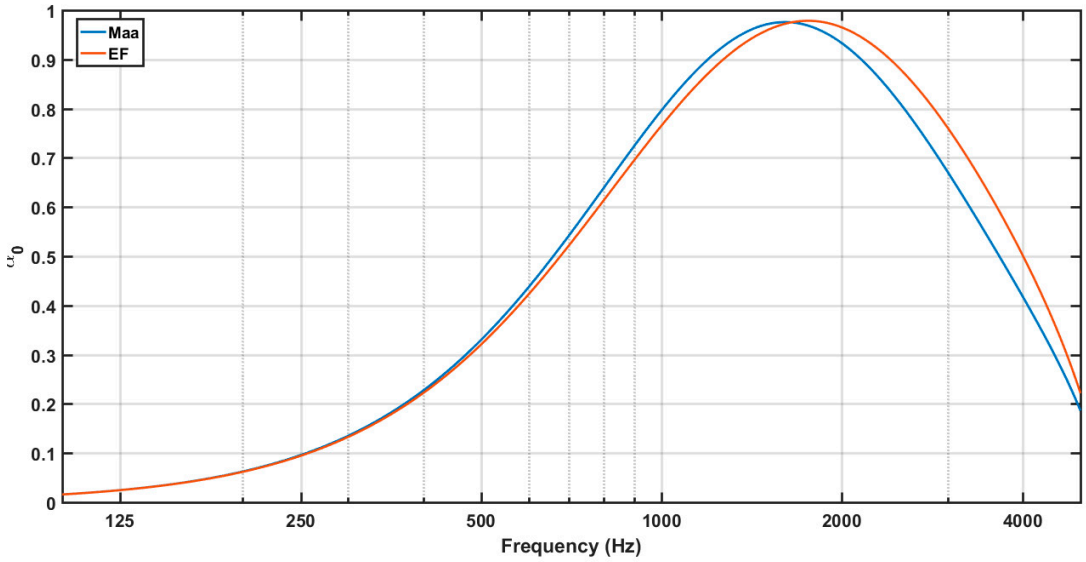

Figure 20. Absorption curves of a SL-MIU with hole perforations, according to the Maa and EF models for (d_1,t_1,ϕ_1,d_2,t_2,ϕ_2,D)=(3 mm,1 mm,10%,41 μm,50 μm,31%,3 cm).

Finally, Ruiz *et al.* [12] compared the experimental absorption curve of a MIU with that predicted by a hybrid model which combined the Maa equation for the carrying panel with the EF equation for the micrometric mesh with excellent results.

2.6. MPP manufactured by infiltration technique

Cobo and Montero de Espinosa [13] proposed to manufacture MPPs by an infiltration technique, which reduces the manufacturing complexity and price. It consists of mixing a polymeric resin with grains of common salt, and curing the mixture into a stove. When the resulting plate is introduced in water, the salt dissolves leaving holes of size determined by those of the grains. The role played by the uniformly sized, evenly distributed holes in a laser drilled MPP, is the same that is played by the irregularly sized, unevenly distributed perforations leaved by the dissolved grain salt in a MPP manufactured by infiltration, Figure 21.

For the case of a MPP with irregularly shaped holes, as those manufactured by infiltration, Cobo and Montero de Espinosa [13] demonstrated that the Maa and the EF models can be still used with some modifications. Firstly, instead the diameter, d, for circular holes, the hydraulic diameter (ratio between four times the surface and the perimeter of the perforations) must be used. For the Maa model, both the resistive and reactive parts of the Maa impedance can be expected to vary slightly due to the irregularity of perforations. Then, the modified Maa impedance was considered

 doi:10.20944/preprints201901.0248.v1

$$Z_{Maa,modified} = a_r R_{Maa} + i a_i X_{Maa}$$
$$R_{Maa} = Re\left\{\frac{i\omega\rho_0 t}{\phi}\left[1-\frac{2}{s\sqrt{-i}}\frac{J_1(s\sqrt{-i})}{J_0(s\sqrt{-i})}\right]^{-1}\right\} + \frac{\sqrt{2\rho_0\omega\eta}}{2\phi} \quad , \quad (27)$$
$$X_{Maa} = Im\left\{\frac{i\omega\rho_0 t}{\phi}\left[1-\frac{2}{s\sqrt{-i}}\frac{J_1(s\sqrt{-i})}{J_0(s\sqrt{-i})}\right]^{-1}\right\} + \frac{0.85\,\rho_0\omega d}{\phi}$$

with (a_r,a_i) real numbers close to 1.

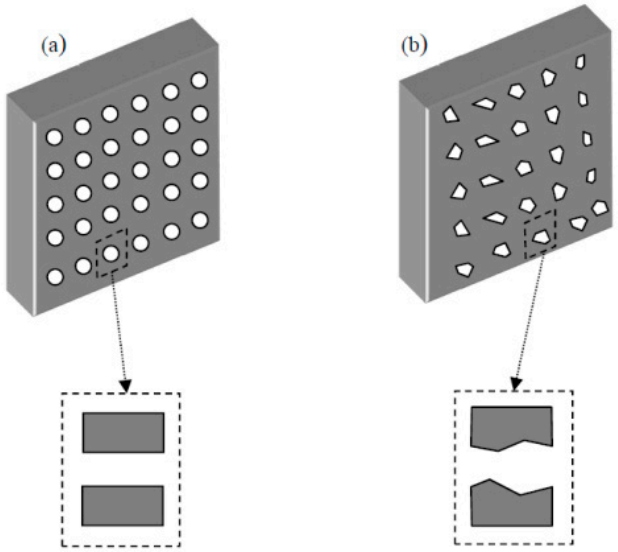

Figure 21. Sketch of a MPP with (a) evenly distributed with regular size holes, and (b) irregular holes unevenly distributed.

For the equivalent fluid model, the irregularity in the perforations could be expected to modify both the flow resistivity and the geometrical tortuosity. Therefore, Cobo and Montero de Espinosa [13] considered the modified resistivity and tortuosity given by

$$\sigma_{modified} = a_\sigma \frac{8\eta}{\phi r^2}$$
$$\alpha_{\infty,modified} = a_{\alpha_\infty}\left[1+\frac{0.85\,d}{t}\left(1-1.14\sqrt{\phi}\right)\right] \quad , \quad (28)$$

where $(a_\sigma, a_{\alpha_\infty})$ are real numbers close to 1.

A MPP was produced by this technique to be measured in an impedance tube with parameters (d,t,ϕ,d)=(0.25 mm,0.25 mm,1%,18mm). The modifying parameters (a_r,a_i, a_σ, a_{α_∞}) resulted to be (1,0.7,1.5,0.7)), respectively. Figure 22 shows the measured and predicted by both models absorption curves for this SL-MPP. The measured absorption curve of the SL-MPP absorber with irregular holes seems to be compatible with a Maa model with unchanged resistance but with a reactance reduced by a 30 %. On the other hand, the fitted factors for the EF model seem to suggest a flow resistivity increased in a 40-50 %, and a geometrical tortuosity decreased in a 30 %. Since the resistivity is inversely proportional to the face velocity of the flow through the MPP [31], an increase of σ can be interpreted as a decrease of this velocity, as a consequence of the irregularly shaped holes. The tortuosity, on the other hand, is shown to be a function of the correction length induced by the radiation of the air column inside the pores in the surrounding media (air in this case) [6]. Therefore, a decreased α_∞ must be interpreted as a shortening of this correction length, due to the irregular holes in this kind of MPPs.

Preprints (www.preprints.org) | NOT PEER-REVIEWED | Posted: 24 January 2019 doi:10.20944/preprints201901.0248.v1

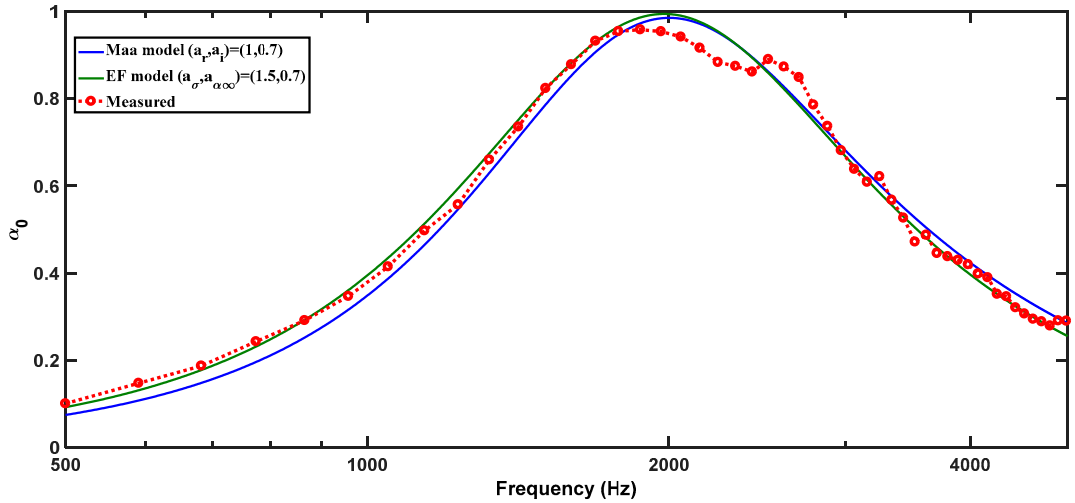

Figure 22. Measured absorption curves of the SL-MPP absorber manufactured by infiltration in comparison with these provided by the modified Maa and EF models.

Ortiz *et al.* [32] demonstrated the capability of SL-MPPs manufactured by infiltration as liners to reduce the tones of an open cavity.

2.7. Absorption of a SL-MPP at Random Incidence

At oblique incidence with angle θ, the input impedance to a SL-MPP, $Z_1(\theta)$, depends on the incidence angle and the type of the panel reaction [33]

$$Z_1(\theta) = \begin{cases} Z_{MPP} - iZ_0 cot(kD) & locally\ reacting \\ Z_{MPP} - i\frac{Z_0 cot(kDcos\theta)}{cos\theta} & bulk\ reacting \end{cases} . \quad (29)$$

A boundary between two media (the air and the MPP surface, in this case) is termed locally reacting when the normal particle velocity at any point of the surface depends only on the local sound pressure at that point and not on the pressure elsewhere [34]. Materials that do not satisfy this condition are said to exhibit bulk reaction [22] or extended reaction [35]. A proper model for bulk reacting boundaries needs to take into account the entire wave field incident on the surface [35]. The reflection and absorption at oblique incidence are

$$R(\theta) = \frac{Z_1 cos\theta - Z_0}{Z_1 cos\theta + Z_0} , \quad (30)$$

$$\alpha(\theta) = 1 - |R(\theta)|^2 . \quad (31)$$

The absorption coefficient at random incidence is [22]

$$\alpha_d = \int_0^{\pi/2} \alpha(\theta) \sin(2\theta)\, d\theta. \quad (32)$$

The random incidence α_d depends on the reaction properties of the boundary. Ingard [36] proposed the notation α_0, α_1 and α_2 for naming the absorption coefficients at normal incidence, random incidence for locally reacting surfaces, and random incidence for bulk reacting surfaces, respectively. Figure 23 shows the absorption coefficients α_0, α_1 and α_2 for a SL-MPP of d=t=0.1 mm, ϕ=1.8%, and an air cavity of D=4 cm. It can be noticed that:

 doi:10.20944/preprints201901.0248.v1

- The random incidence absorption coefficient of a locally reacting SL-MPP has an absorption bandwidth rather similar to the normal incidence absorption coefficient, and a slight reduction of the peak absorption.
- The random incidence absorption coefficient of a bulk reacting SL-MPP has an absorption curve quite displaced towards higher frequencies as compared to the normal incidence absorption coefficient, with a more reduced absorption peak.

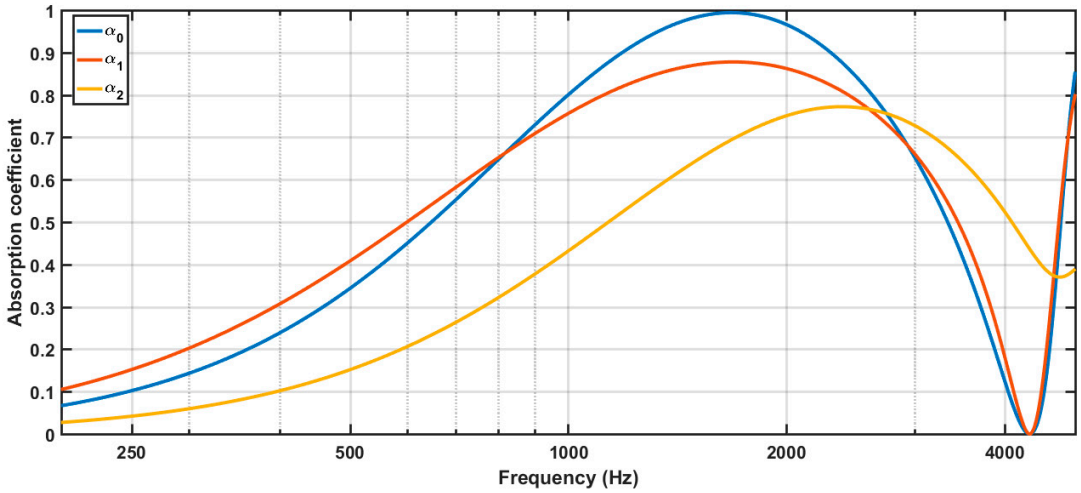

Figure 23. Absorption coefficients at normal (α_0) and random incidence for local (α_1) and bulk (α_2) reaction for a SL-MPP with parameters (d,t,ϕ,D)=(0.1 mm,0.1 mm, 1.8%, 4 cm).

It is usual to design MPPs at normal incidence, since the mathematical problem is much simpler. However, the designed MPP will likely have to perform at diffuse field. The bandwidth of the designed normal incidence SL-MPP will be similar to that of the random incidence provided that the interface is working as a local reaction surface. This can be easily achieved if the air cavity is properly partitioned, for example with a honeycomb structure.

3. Multiple-layer MPP (ML-MPP)

Therefore, the SL-MPP first proposed by Maa [2-3] is a good alternative to fibrous and porous materials under special conditions of clean and health requirements [37]. Its absorption bandwidth, however, is limited to 1-2 octaves or even slightly superior to two octaves for ultraperforated MPPs [14]. As an example, Figure 24 shows the absorption curve of such an ultraperforated MPP with (d,t,ϕ,D)=(0.12 mm,1 mm,10%,2 cm), which provides absorption in a band of almost 2.3 octaves.

To increase the absorption bandwidth, Maa [2], Lee and Swenson [15], and Lee and Kwon [16] proposed the design of ML-MPPs. Maa [2] and Lee y Swenson [15] calculated the absorption coefficient applying the equivalent circuit technique. Lee and Kwon [16], on the other hand, applied the impedance transfer method. Cobo *et al.* [17] demonstrated that both techniques provide different results, being the impedance transfer method the correct one. The impedance transfer method is applied in the following to analyse two ML-MPPs.

Preprints (www.preprints.org) | NOT PEER-REVIEWED | Posted: 24 January 2019 doi:10.20944/preprints201901.0248.v1

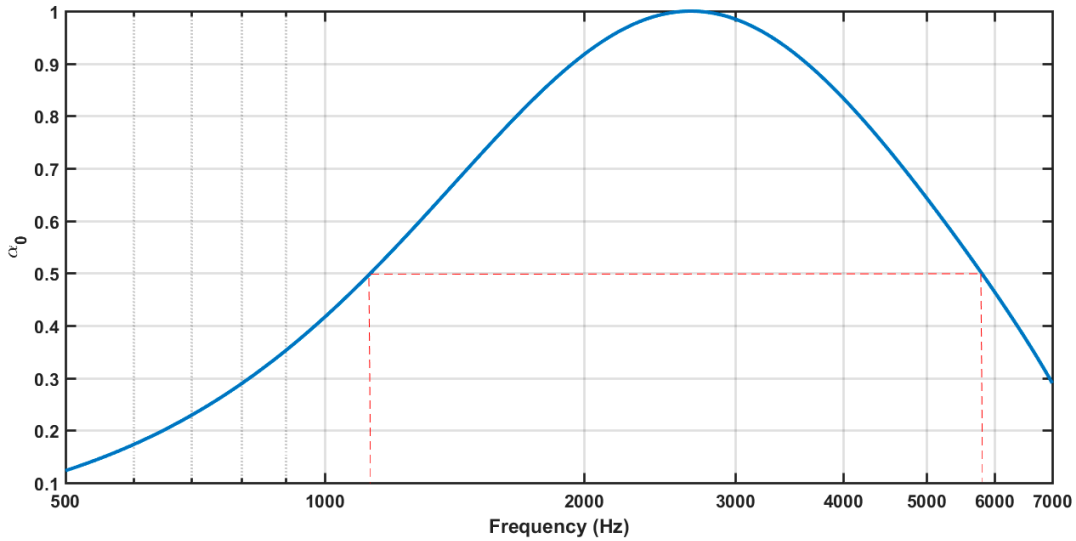

Figure 24. Normal incidence absorption coefficient of a SL-MPP with d=0.12 mm, t=1 mm, ϕ=10 %, and D=2 cm.

3.1. Double-layer MPP (DL-MPP)

Figure 25 displays the sketch of the DL-MPP at normal incidence. It consists of two MPPs of impedances Z_{m1} and Z_{m2} with to air cavities of impedances Z_{c1} and Z_{c2}. The input impedances to the two interfaces are Z_1 and Z_2. Also, the characteristic impedance of the air is Z_0. Sound waves attain the DL-MPP system from the left at normal incidence.

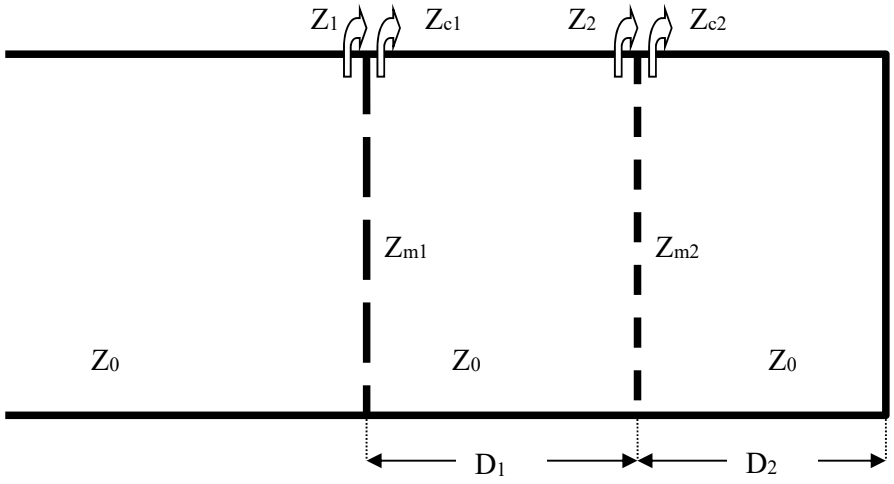

Figure 25. Sketch of a DL-MPP at normal incidence.

The input impedance to the DL-MPP system is

$$Z_1 = Z_{m1} + Z_0 \frac{Z_2 cos(kD_1) + iZ_0 sin(kD_1)}{Z_0 cos(kD_1) + iZ_2 sin(kD_1)} \quad , \tag{33}$$

with

$$Z_2 = Z_{m2} - iZ_0 cot(kD_2) \quad . \tag{34}$$

Preprints (www.preprints.org) | NOT PEER-REVIEWED | Posted: 24 January 2019 doi:10.20944/preprints201901.0248.v1

Eqs. (33-34) together with Eqs. (1-2) allows to obtain the absorption coefficient of a DL-MPP at normal incidence. Therefore, the absorption of a DL-MPP depends on 8 constitutive and geometrical parameters of the MPPs, namely (t_1,d_1,ϕ_1,D_1,t_2,d_2,ϕ_2,D_2). As an example, Figure 26 shows the absorption coefficient of a DL-MPP for the combination of parameters (t_1,d_1,ϕ_1,D_1,t_2,d_2,ϕ_2,D_2)=(0.15 mm,1 mm,10%,2 cm,0.15 mm,1 mm,15%,2 cm). The absorption bandwidth, obtained by Eq. (14), is 3.24 octaves.

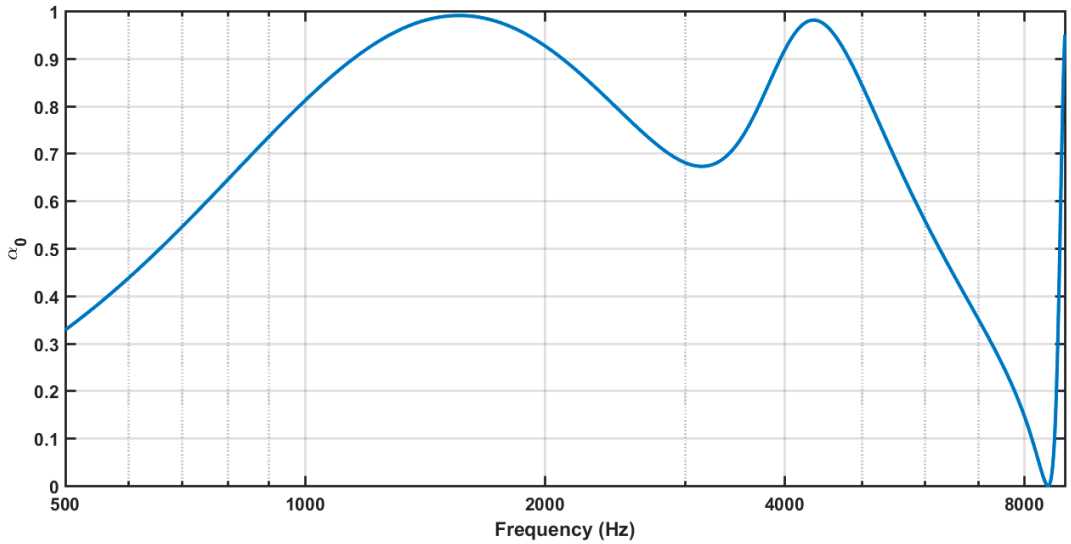

Figure 26. Normal incidence absorption coefficient of a DL-MPP with (d_1,t_1,ϕ_1,D_1,d_2,t_2,ϕ_2,D_2)=(0.15 mm,1 mm,10%,2 cm,0.15 mm,1 mm,15%,2 cm).

Since the acoustic performance of a DL-MPP depends on 8 parameters, it is difficult to know a priori the combination of these parameters affording the maximum absorption within a prescribed frequency band. Ruiz *et al.* [18] demonstrated that the combination of the 8 parameters of a DL-MPP can be optimised by Simulated Annealing.

3.2. Triple-layer MPP (TL-MPP)

Figure 27 shows the sketch of the TL-MPP at normal incidence. It consists of three MPPs of impedances Z_{m1}, Z_{m2} and Z_{m3} with three air cavities of impedances Z_{c1}, Z_{c2} and Z_{c3}. The input impedances to the three interfaces are Z_1, Z_2 and Z_3. Also, the characteristic impedance of the air is Z_0. Sound waves reach the TL-MPP system from the left at normal incidence.

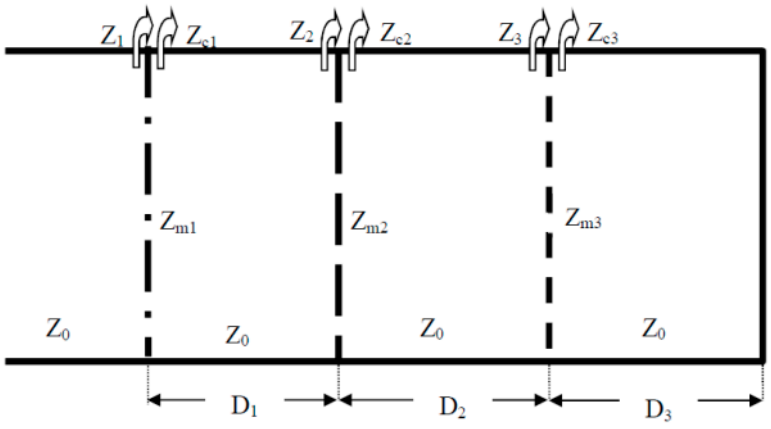

Figure 27. Sketch of a TL-MPP at normal incidence.

Preprints (www.preprints.org) | NOT PEER-REVIEWED | Posted: 24 January 2019 doi:10.20944/preprints201901.0248.v1

The transfer impedance method provides the following equations for the input impedance

$$Z_1 = Z_{m1} + Z_0 \frac{Z_2 cos(kD_1) + iZ_0 sin(kD_1)}{Z_0 cos(kD_1) + iZ_2 sin(kD_1)} \quad . \tag{35}$$

where

$$Z_2 = Z_{m1} + Z_0 \frac{Z_3 cos(kD_2) + iZ_0 sin(kD_2)}{Z_0 cos(kD_2) + iZ_3 sin(kD_2)} \quad , \tag{36}$$

and

$$Z_3 = Z_{m3} - iZ_0 cot(kD_3) \quad . \tag{37}$$

The normal incidence absorption coefficient of a TL-MPP depends on 12 constitutive and geometric parameters (d_1,t_1,ϕ_1,D_1,d_2,t_2,ϕ_2,D_2,d_3,t_3,ϕ_3,D_3). To illustrate the capability of TL-MPP to provide broadband absorption, Figure 28 shows the normal incidence absorption coefficient of such absorber for the combination of parameters (d_1,t_1,ϕ_1,D_1,d_2,t_2,ϕ_2,D_2,d_3,t_3,ϕ_3,D_3)=(0.15 mm,1.35,15%,0.89 cm,0.15 mm,1.4 mm,10%,1.3 cm,0.15 mm,1.1 mm,5%,2 cm). Notice that this TL-MPP provides absorption in a band of 4.25 octaves with a total thickness D_1+D_2+D_3=4.6 cm.

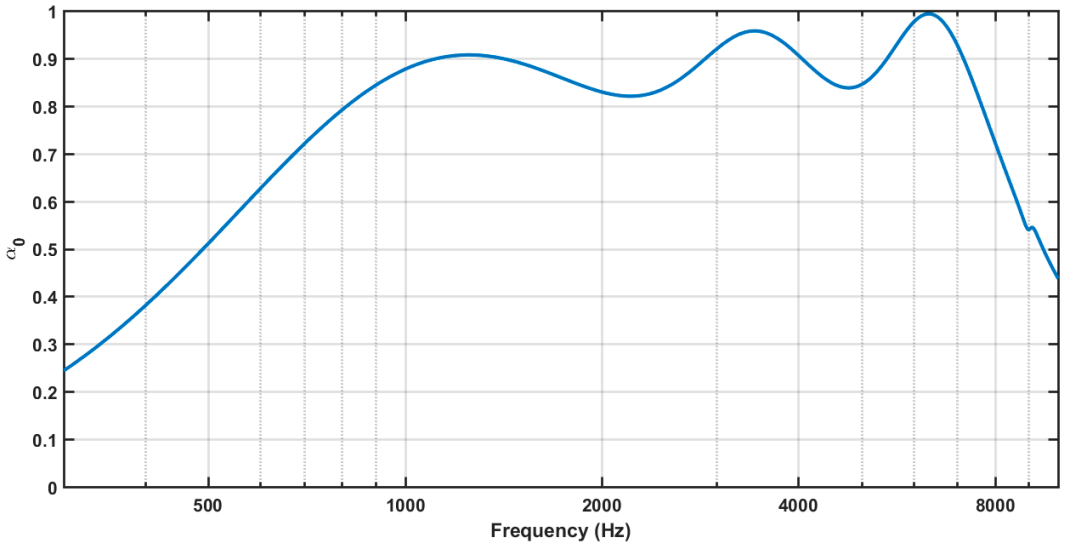

Figure 28. Normal incidence absorption coefficient of a TL-MPP with parameters (d_1,t_1,ϕ_1,D_1,d_2,t_2,ϕ_2,D_2,d_3,t_3,ϕ_3,D_3)=(0.15 mm,1.35,15%,0.89 cm,0.15 mm,1.4 mm,10%,1.3 cm,0.15 mm,1.1 mm,5%,2 cm).

Cobo *et al.* [38] confirmed that it is possible to manufacture cheap, optimised by Simulated Annealing, TL-MPPs by drilling epoxy laminates primarily used for advanced circuitry applications.

4. Conclusions

Sound absorbers based on MPPs were proposed as a good alternative to conventional porous/fibrous absorbers when high demanding clean and health aspects are required. The mathematical bases for designing such absorbers were already posed by Maa in the last quarter of the 20 century. However, its development as large scale absorbers has taken a lot of time due mainly to two reasons: its low absorption bandwidth and its high manufacturing cost. These limitations are

nowadays getting over. Modern MPPs can be manufactured by 3D printing or by drilling epoxy laminates primarily used for advanced circuitry. The absorption bandwidth can be significantly increased by designing multiple-layer MPPs. Specifically, the sound absorption of a MPP can be increased from roughly two octaves, for a single-layer MPP, to more than three octaves, for double-layer MPP, and more than four octaves, with a triple-layer MPP. These bandwidths are enough to cover most of the absorption needs in building acoustics.

Author Contributions: conceptualization, methodology, and first draft preparation P.C.; conceptualization, methodology and revision of first draft F.S.

Funding: This research was funded by the Ministry of Science, Innovation and University through grant number DPI2016-79559R.

Acknowledgments: Fruitful discussions with C. de la Colina are acknowledged.

Conflicts of Interest: The authors declare no conflict of interest

References

1. Cobo, P., Ruiz, H., Alvarez, J. Double-Layer Microperforated Panel/Porous absorber as liner for anechoic closing of the test section in wind tunnels**.** *Acta Acustica united with Acustica* **2010**, *96*, 914-922.
2. Maa, D.Y. Microperforated-panel wideband absorbers. *Noise Control Eng J* **1987**, *29*, 77-84.
3. Maa, D.Y. Potential of microperforated panel absorber. *J Acoust Soc Am* **1998**, *104*, 2861-2866.
4. Allard, J.F. ***Propagation of Sound in Porous Media. Modelling Sound Absorbing Materials.*** Elsevier Applied Science, London, UK, 1993.
5. Allard, J.F., Atalla, N. ***Propagation of Sound in Porous Media. Modelling Sound Absorbing Materials.*** John Wiley & Sons, Chichester, West Sussex, UK, 2009.
6. Atalla, N., Sgard, J.F. Modeling of perforated plates and screens using rigid frame porous models. *J Sound Vib* **2007**, *303*, 195-208.
7. Ingard, U. On the theory and design of acoustic resonators. *J Acoust Soc Am* **1953** *25*, 1037-1061.
8. Maa, D.Y. Theory of microslit absorbers. *Chinese J Acoust* **2001**, *20*, 1-10.
9. Randeberg, R.T. Perforated panel absorbers with viscous energy dissipation enhanced by orifice design. Doctoral Thesis, Norweian University of Science and Technology, Trondheim, 2000.
10. Vigran, T.O., Pettersen, O.K.Ø. The absorption of slotted panels revisited. Forum Acusticum, Budapest (Hungary), **2005**, 2037-2040.
11. Pfretzschner, J., Cobo, P., Simon, F., Cuesta, M., Fernández, A. Microperforated Insertion Units: an alternative strategy the design of microperforated panels. *Appl Acoust* **2006**, *67*, 62-73.
12. Ruiz, H., Cobo, P., Dupont, T., Martin, B., Leclaire, Ph. Acoustic properties of plates with unevenly distributed macroperforations backed by woven meshes. *J Acoust Soc Am* **2012**, *132*, 3138-3147.
13. Cobo, P., Montero de Espinosa, F. A proposal of cheap microperforated panels manufactured by infiltration. *Appl Acoust* **2013**, *74*, 1069-1075.
14. Quian, Y.J., Kong, D.Y., Liu, S.M., Sun, S.M., Xhao, Z. Investigation on micro-perforated panel absorber with ultra-micro perforations. *Appl Acoust* **2013**, *74*, 931-935.
15. Lee, J., Swenson Jr., G.W. Compact sound absorbers for low frequencies. *Noise Con Eng J* **1992**, *38*, 109-117.
16. Lee, D.H., Kwon, Y.P. Estimation of the absorption performance of multiple layer perforated panel systems by transfer matrix method. *J Sound Vib* **2004**, *278*, 847-860.
17. Cobo, P., Cuesta, M., Siguero, M. Comparison of models describing double layer microperforated absorbers. *Noise Cont Eng J* **2009**, *57*, 10-15.
18. Ruiz, H., Cobo, P., Jacobsen, F. Optimization of multiple-layer microperforated panels by simulated aneealing. *Appl Acoust* **2011**, *72*, 772-776.
19. Jaouen, L., Becot, F.X. Acoustical characterization of perforated facings. *J Acoust Soc Am* **2011**, *129*, 1400-1406.
20. Tayong, R., Leclaire, P. Hole interaction effects under high and medium sound intensities for micro-perforated panels design. 10éme Congress Francais d'Acoustique **2010**, Lyon.
21. Cobo, P. ***Absorción del Sonido***. Biblioteca de Ciencias, 42, CSIC, Madrid, Spain, 2015.
22. Fahy, F. ***Foundations of Engineering Acoustics***. Academicc Press, San Diego, USA, 2001.

575 23. Hou, K. Measurement and modeling of micro-perforated panels. Master Thesis, Purdue University, West
576 Lafayette, Indiana, USA, 2009.
577 24. Melling, T.H. The acoustic impedance of perforates at medium and high sound pressure levels. *J Sound Vib*
578 **1973**, *29*, 1-65.
579 25. Rschevkin, S.N. ***A Course of Lectures on the Theory of Sound***. Pergamon Press, Oxford, UK, 1963.
580 26. Stinson, M.R., Champoux, Y. Propagation of sound and the assignment of shape factors in models of
581 porous materials having simple geometries. *J Acoust Soc Am* **1992**, *91*, 685-695.
582 27. Cobo, P., Pfretszchner, J., Cuesta, M., Anthony, D.K. Hybrid passive-active absorption using
583 microperforated panels. *J Acoust Soc Am* **2004**, *116*, 2118-2125.
584 28. Cobo, P., Fernández, A. Hybrid passive-active absorption of broadband noise using MPPs. *Noise*
585 *&Vibration Worldwide* **2006**, *37*, 19-23.
586 29. Cobo, P., Cuesta, M. Hybrid passive-active absorption of a microperforated panel in free field conditions. *J*
587 *Acoust Soc Am* **2007**, *121*, EL251-EL255.
588 30. Cobo, P., Cuesta, M. Measuring hybrid passive-active sound absorption of a microperforated liner at
589 oblique incidence. *J Acoust Soc Am* **2009**, *125*, 185-190.
590 31. Mechel, F.P, Ver I.L. Sound absorbing materials and sound absorbers. In ***Noise and Vibration Control***
591 ***Engineering*** (Beranek LL, Ver IL, Eds.). John Wiley & Sons, New York, USA, 1992.
592 32. Ortiz, S., González, C., Cobo, P., Montero de Espinosa, F. Attenuating open cavity tones by lining its walls
593 with microperforated panels. *Noise Con Eng J* **2014**, *62*, 145-151.
594 33. Mechel, F.P. ***Formulas of Acoustics***. Spriger-Verlag, Berlin, Germany, 2002.
595 34. Morfey, C.L. ***Dictionary of Acoustics***. Academic Press. London, UK, 2001
596 35. Cox, T.J., D'Antonio, P. ***Acoustic Absorbers and Diffusers. Theory, Design, and Application***. Spon Press,
597 New York, USA; 2004.
598 36. Ingard, U. ***Notes on Sound Absorption***. Kittery Point, Maine, USA, 1999.
599 37. Kang, J., Fuchs, H.V. Predicting the sound absorption of open weave textiles and microperforated
600 membranes backed by an air space. *J Sound Vib* **1999**, *220*, 905-920.
601 38. Cobo, P., de la Colina, C., Roibás, E., Chimeno, M., Simón, F. A wideband triple-layer microperforated
602 panel sound absorber. Submitted to *Composite Structures* **2019**.

603